

A RARE EARLY-TYPE STAR REVEALED IN THE WING OF THE SMALL MAGELLANIC CLOUD

C. J. EVANS¹, R. HAINICH², L. M. OSKINOVA², J. S. GALLAGHER III³, Y.-H. CHU⁴,
R. A. GRUENDL⁴, W.-R. HAMANN², V. HÉNAULT-BRUNET⁵ AND H. TODT²

Received; Accepted

ABSTRACT

Sk 183 is the visually-brightest star in the N90 nebula, a young star-forming region in the Wing of the Small Magellanic Cloud (SMC). We present new optical spectroscopy from the Very Large Telescope which reveals Sk 183 to be one of the most massive O-type stars in the SMC. Classified as an O3-type dwarf on the basis of its nitrogen spectrum, the star also displays broadened He I absorption which suggests a later type. We propose that Sk 183 has a composite spectrum and that it is similar to another star in the SMC, MPG 324. This brings the number of rare O2- and O3-type stars known in the whole of the SMC to a mere four. We estimate physical parameters for Sk 183 from analysis of its spectrum. For a single-star model, we estimate an effective temperature of 46 ± 2 kK, a low mass-loss rate of $\sim 10^{-7} M_{\odot} \text{ yr}^{-1}$, and a spectroscopic mass of $46^{+9}_{-8} M_{\odot}$ (for an adopted distance modulus of 18.7 mag to the young population in the SMC Wing). An illustrative binary model requires a slightly hotter temperature (~ 47.5 kK) for the primary component. In either scenario, Sk 183 is the earliest-type star known in N90 and will therefore be the dominant source of hydrogen-ionising photons. This suggests Sk 183 is the primary influence on the star formation along the inner edge of the nebula.

Subject headings: open clusters and associations: individual (N90; NGC 602) — stars: early-type — stars: fundamental parameters — stars: individual (Sanduleak 183)

1. INTRODUCTION

The Magellanic Clouds provide an excellent example of interacting, metal-poor dwarf galaxies on our own doorstep, with neutral hydrogen maps revealing large structures such as the Magellanic Bridge (which connects the Clouds), and the extensive Magellanic Stream and Leading Arm (e.g., Putman 2000). The Bridge is linked to the eastern side of the Small Magellanic Cloud (SMC) by an extended ‘Wing’, which has a lower content of gas, dust and stars than the main body of the SMC, suggesting it should be unfavourable to star formation. However, the young stellar cluster NGC 602 presents spectacular evidence to the contrary, with a star-formation rate which appears comparable to well-studied Galactic regions (e.g. Cignoni et al. 2009).

NGC 602 is a loose term for a rich region comprising at least three distinct clusters (Westerlund, 1964). NGC 602a⁶ is embedded in the N90 emission nebula (Henize, 1956), NGC 602b is a closely-related, smaller cluster approximately 1.5 to the north, and NGC 602c is $\sim 11'$ to the northeast. Other nearby H α emission regions include N88 and N89 (Lindsay 104) which, together with NGC 602, are associated with the only H α supergiant shell known in the SMC (‘SGS-SMC1’, Meaburn, 1980).

Optical imaging of NGC 602a from the *Hubble Space Telescope* (*HST*) Advanced Camera for Surveys (ACS) is particularly striking⁷, engendering the popular moniker of the ‘Hubble Bubble’. The *HST* observations and deep infrared images from the *Spitzer Space Telescope* have given us an exquisite view of the stellar content and star formation in NGC 602a and N90 (Carlson et al. 2007, 2011; Gouliermis et al. 2007; Schmalzl et al. 2008; Nigra et al. 2008; Cignoni et al. 2009).

As part of a new study of SGS-SMC1 we have obtained optical spectroscopy of its luminous stellar population with the Very Large Telescope (VLT). In the course of the program we observed Sk 183 (Sanduleak, 1969)⁸, the visually brightest star in the N90 nebula (see Figure 1). In this article we present the classification and analysis of these observations, which reveal it to be one of the most massive O-type stars in the SMC.

2. SPECTROSCOPY

Optical spectroscopy was obtained on 2010 October 24-26 with the VLT FLAMES instrument (Pasquini et al. 2002), as summarised in Table 1. Sk 183 was observed as part of the larger survey of the region with the Medusa-fibre mode of FLAMES, using three of the standard settings of the Giraffe spectrograph: LR02, LR03, and HR15N, delivering spectral resolving powers of 7000, 8500, and 16 000, respectively (e.g. Evans et al. 2011). Individual exposure times were 1800s for all settings.

The ESO Common Pipeline Library FLAMES reduction routines (v.2.8.7) were used for the standard processing stages, i.e. bias subtraction, fibre location, summed extractions, division by a normalized flat-field, and wave-

¹ UK Astronomy Technology Centre, Royal Observatory Edinburgh, Blackford Hill, Edinburgh, EH9 3HJ, UK

² Institute for Physics and Astronomy, University of Potsdam, 14476 Potsdam, Germany

³ Department of Astronomy, University of Wisconsin-Madison, 5534 Sterling, 475 North Charter St., Madison, WI 53706, USA

⁴ Astronomy Department, University of Illinois, 1002 W. Green Street, Urbana, IL 61801, USA

⁵ Scottish Universities Physics Alliance (SUPA), Institute for Astronomy, University of Edinburgh, Royal Observatory Edinburgh, Blackford Hill, Edinburgh, EH9 3HJ, UK

⁶ Cluster 105 from Lindsay (1958)

⁷ <http://hubblesite.org/newscenter/archive/releases/2007/04/>

⁸ $\alpha = 01^{\text{h}} 29^{\text{m}} 24^{\text{s}}.6$, $\delta = -73^{\circ} 33' 16''.43$, J2000. Aliases include: NGC 602a #15 (Westerlund, 1964); NGC 602 #8 (Hutchings et al. 1991); SMC 83235 (Massey, 2002).

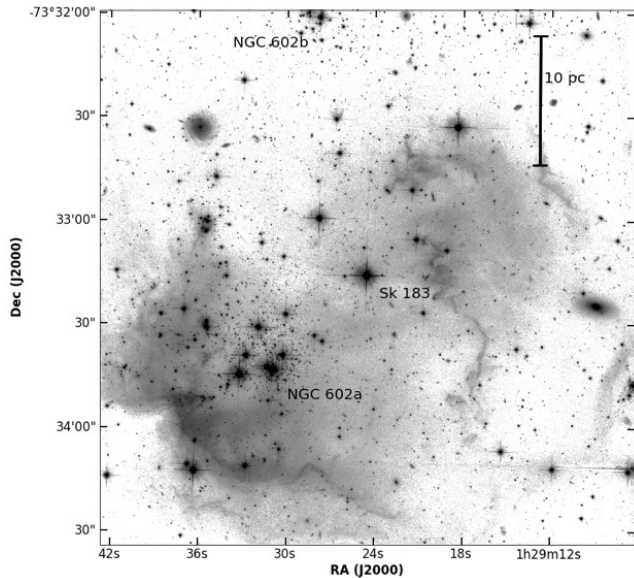


Figure 1. *HST*-ACS *F814W* image of NGC 602a and its associated H II region (N90), centred on Sk 183. NGC 602b is approximately 1.5 to the north. The 10 pc scale assumes the ‘short’ distance modulus of 18.7 mag (see Section 3.1).

length calibration. The spectra were then corrected to the heliocentric frame, and a median sky spectrum was subtracted (for more details see Evans et al. 2011).

Qualitative inspection of the spectra revealed no evidence of radial velocity variations associated with binarity, further supported by the measurements in Section 2.2. Thus, the spectra from each exposure/setting were co-added, yielding a signal-to-noise ratio in excess of 250 per rebinned pixel from the pipeline. However, note that the observations only spanned three nights, so our detection sensitivity to radial velocity variations from anything but a short-period companion will have been low.

There are archival, low-dispersion observations of Sk 183 from the *International Ultraviolet Explorer (IUE)* from Hutchings et al. (1991). Although at low resolution, the lack of strong UV emission-lines is evident (see Figure 4 from Hutchings et al.), consistent with the weak wind-profiles seen in other massive stars in the SMC, e.g. Walborn et al. (1995, 2000).

2.1. Spectral Classification

The $\lambda\lambda 3950\text{--}4750\text{ \AA}$ region of the spectra of Sk 183 is shown in Figure 2, in which the data have been smoothed and rebinned to an equivalent resolving power of $R = 4000$ for classification (cf. the new Galactic atlas of standards from Sana et al. in preparation). Although relatively modest in strength, N IV $\lambda 4058$ emission has an intensity comparable to that from N III $\lambda\lambda 4634\text{--}41\text{--}42$. Employing the criteria from Walborn et al. (2002), this suggests a classification of O3 V((f*))z, in which the ‘z’ suffix indicates that the $\lambda 4686$ absorption has a greater depth than any of the other helium lines (Walborn & Blades, 1997; Walborn 2009).

An early-type classification is supported by the weak absorption from Nv ($\lambda\lambda 4604, 4620$), but there are other features which are not fully consistent with the O3 classification. For instance, the apparent intensities of the

Table 1
Summary of VLT-FLAMES spectroscopy of Sk 183

Setting	Date	Exp. Time [s]	λ -coverage [\AA]	R
LR02	2010-10-24	7×1800	3960-4564	7000
	2010-10-26	2×1800		
LR03	2010-10-25	4×1800	4499-5071	8500
HR15N	2010-10-25	2×1800	6442-6817	16000

Note. — The final column gives the effective resolving power (R) at the central wavelength of each setting.

He I $\lambda\lambda 4388, 4471, 4713$ lines suggest a later spectral type. The intensity of the He II $\lambda 4026$ absorption is also relatively strong for an O3 type dwarf, but may be explained by a contribution from He I. We note that Hutchings et al. (1991) classified their low-dispersion optical spectrum of Sk 183 as O6, but the lack of strong He I $\lambda 4471$ absorption in their data argues for an earlier type.

As a possible explanation of the spectral properties of Sk 183 we propose that its spectrum is composite in nature, and results either from a binary system or an unresolved multiple. While the star appears as a single point source in the image from the *HST* ACS, the spatial resolution in the Wide Field Channel (2 pixels = $0''.1$) subtends several thousand AU at the distance of the SMC. The composite character of the Sk 183 spectrum is further supported by the morphology of the He I absorption, which indicates rapid rotation in a secondary component (e.g. $\lambda 4388$ in Figure 2) or perhaps evidence for further multiplicity. Without additional data (e.g., time-series photometry or multi-epoch spectroscopy) it is hard to constrain the nature of Sk 183 further and we adopt a classification of O3 V((f*))z + OB. Similar composite classifications were employed for three objects by Walborn et al. (2002), who demonstrated that one (Cyg OB2-22) was indeed a composite of an O3 supergiant and an O6 dwarf.

Circumstantial evidence for the composite nature of Sk 183 is also provided by the spectra of another star in the SMC, MPG 324 (Massey et al. 1989)⁹, previously classified as an O4 dwarf (Niemela et al. 1986; Massey et al. 1989; Walborn et al. 1995, 2000; Evans et al. 2006). Returning to the FLAMES spectra of MPG 324 from Evans et al. (2006), similar features are seen as those in Sk 183, i.e., N IV emission indicative of an early (<O4) type, combined with He I absorption suggesting a later type (see Figure 2). Indeed, Evans et al. (2006) noted MPG 324 as a single-lined binary due to a $\sim 30\text{ km s}^{-1}$ shift in the He II $\lambda 4542$ line between two epochs of observations with one of the FLAMES settings. The He I $\lambda 4471$ line in these two epochs was contaminated by nebular emission, but the wings of the profile were (qualitatively) consistent with a zero velocity shift, suggesting a potentially different origin to the He II absorption. We reclassify MPG 324 as O3 V((f*))z + OB, and note that Massey et al. (2009) classified MPG 324 as O5 V in the course of their atmospheric analysis – they did not see N III emission in their (lower-resolution) spectrum, but N IV emission remains at $\lambda 4058$, which argues for an earlier type.

⁹ Aliases: NGC 346 #6 (Walborn et al. 1995); NGC 346 007 (Evans et al. 2006).

The use of an O3 type to describe both Sk 183 and MPG 324 arises from the high-quality of the spectra, in which the N IV emission is clearly seen. These classifications are based on the spectroscopic framework in this regime of massive stars, which have unambiguous criteria linked to the relative intensities of the nitrogen lines (Walborn et al. 2002, 2004; Sota et al. 2011).

2.2. Stellar Radial Velocities

Stellar radial velocities (v_r) for Sk 183 were determined from Gaussian fits to the He II $\lambda\lambda 4200, 4542$ lines. From measurements of each LR02 observation we found weighted means of $v_r = 162.5 \pm 1.2$ and $162.4 \pm 0.8 \text{ km s}^{-1}$ from He II $\lambda 4200$ and $\lambda 4542$, respectively. The quoted errors are $1\text{-}\sigma$ uncertainties on the positions of the centroids of the fits. A statistical variability analysis of the individual radial velocity measurements does not detect significant differences, suggesting a constant velocity from our spectroscopy. From fits to the superimposed H α and [O III] $\lambda\lambda 4959, 5007$ nebular emission, the mean gas velocity is slightly offset with $v_{\text{gas}} = 172.1 \pm 1.1 \text{ km s}^{-1}$. This is approximately 5 km s^{-1} lower than the gas velocity measured at the same right ascension (but $\sim 20''$ further south) by Nigra et al. (2008).

3. PHYSICAL PROPERTIES OF SK 183

3.1. Distance and Extinction

The distance to Sk 183 is the largest uncertainty on its total luminosity. Given the long-standing questions regarding the depth and structure of the SMC, the ‘standard’ distance modulus of $\sim 18.9 \text{ mag}$ (e.g. Harries et al. 2003) might not be appropriate for the Wing. There is mounting evidence for objects in the eastern part of the SMC to suggest shorter distances, e.g., Howarth (1982), Mathewson et al. (1986), Crowl et al. (2001), and Glatt et al. (2008). Indeed, in their analysis of the *HST* imaging, Cignoni et al. (2009) advocate a distance modulus to the young population in NGC 602 of 18.7 mag.

Sk 183 is relatively isolated from bright companions so, to determine the line-of-sight reddening, optical *UBVR* photometry was taken from Massey (2002). We also employed the *F814W* magnitude from Schmalzl et al. (2008) and near-infrared *JHK_s* magnitudes from the Two Micron All Sky Survey (2MASS; Skrutskie et al. 2006), as shown in Figure 3 and summarised in Table 2. Photometry of Sk 183 at longer wavelengths has become available recently from the *Wide-field Infrared Survey Explorer* (*WISE*, Wright et al. 2010); these data are discussed separately in Section 4.2.

From fits of the adopted model atmosphere (Section 3.2) to the spectral energy distribution of the *IUE* spectroscopy and multi-band photometry (Figure 3) we derived $E(B - V) = 0.09 \pm 0.01 \text{ mag}$. This included contributions from both internal SMC and foreground Galactic reddening, taking the lower bound of $E(B - V) = 0.04 \text{ mag}$ from Bessell (1991) for the latter. In calculating the total visual extinction we adopted ratios of total-to-selective extinction of 3.1 (Galactic; Howarth, 1983) and 2.7 (SMC; Bouchet et al. 1985), leading to $A_V = 0.26 \text{ mag}$ and an absolute magnitude of $M_V = -5.14$ or -5.34 mag (for distance moduli of 18.7 and 18.9 mag, respectively). Such values are at the faint

Table 2
Photometry of Sk 183

Band	Magnitude	Ref.
<i>U</i>	$12.51 \pm 0.01^\dagger$	Massey (2002)
<i>B</i>	$13.59 \pm 0.01^\dagger$	Massey (2002)
<i>V</i>	13.82 ± 0.01	Massey (2002)
<i>R</i>	$13.89 \pm 0.02^\dagger$	Massey (2002)
<i>F814W</i>	14.128 ± 0.003	Schmalzl et al. (2008)
<i>J</i>	14.426 ± 0.029	2MASS
<i>H</i>	14.606 ± 0.063	2MASS
<i>K_s</i>	14.618 ± 0.091	2MASS
<i>W1</i> (3.4 μm)	14.480 ± 0.029	<i>WISE</i>
<i>W2</i> (4.6 μm)	14.255 ± 0.041	<i>WISE</i>
<i>W3</i> (12 μm)	10.368 ± 0.043	<i>WISE</i>
<i>W4</i> (22 μm)	5.955 ± 0.031	<i>WISE</i>

Note. — † Calculated in quadrature from the errors quoted on the colours by Massey (2002).

end of those found for early-type dwarfs (e.g. Walborn et al. 2002), and are comparable to others classified as VZ (see, e.g., Figure 4 from Walborn 2009), notwithstanding a potential contribution from a companion.

3.2. Atmospheric Analysis

3.2.1. PoWR Models

Physical properties for Sk 183 were estimated from comparisons of the FLAMES data with synthetic spectra calculated with the PoWR code (e.g. Hamann & Gräfener, 2003; 2004). PoWR treats the wind and the photosphere self-consistently and has been used to analyse the wind characteristics of O-type stars (Oskinova et al. 2006, 2007), helium-rich subdwarf O-type stars (Jeffery & Hamann, 2010), and B-type main-sequence stars (Oskinova et al. 2011)¹⁰.

In brief, the PoWR code solves the radiative transfer equation for a spherically-expanding atmosphere and the statistical equilibrium equations simultaneously, while also accounting for energy conservation and allowing deviations from local thermodynamic equilibrium (i.e. non-LTE). A PoWR model is defined by its effective temperature (T_{eff}), effective surface gravity ($\log g_{\text{eff}}$), luminosity (L), mass-loss rate (\dot{M}), terminal velocity of the wind (v_∞), and chemical composition. A standard β -velocity law ($\beta = 1$) for the wind acceleration was assumed in all calculations; the density follows from the velocity via the mass-continuity equation. The wind domain is smoothly connected to the photosphere, at which point the hydrostatic equilibrium is approached asymptotically.

The models included transitions of hydrogen, helium, carbon, oxygen, nitrogen, and silicon. Iron and iron-group elements were included using the concept of superlevels, as described by Gräfener et al. (2002); this is important because of the blanketing effect of the summed opacities on the atmospheric structure.

3.2.2. ‘Single-star’ Analysis

We first assumed that the observed spectrum originates from a single star. Stellar parameters were de-

¹⁰ Analogous to, e.g., the differences discussed by Rivero González et al. (2011) between results from CMFGEN (Hillier & Miller, 1998) and FASTWIND (Puls et al. 2005), we note there may be small systematic differences if the parameters determined from PoWR were compared to those obtained with other codes.

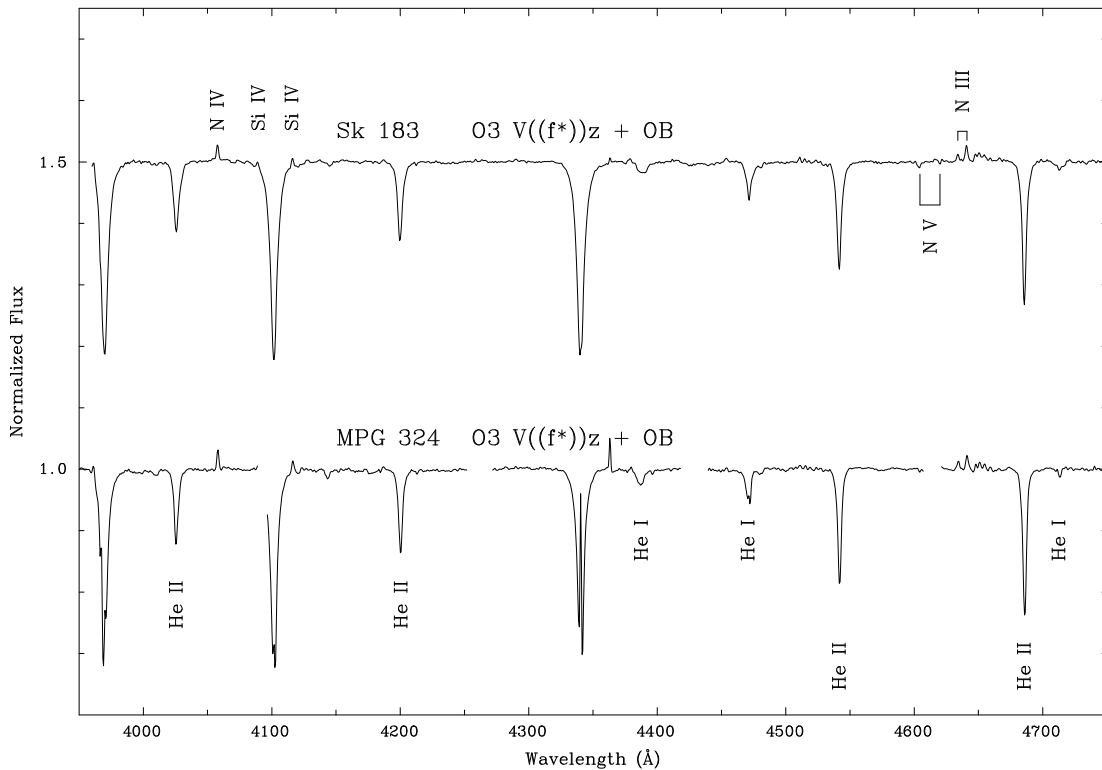


Figure 2. Combined FLAMES spectrum of Sk 183 together with that of NGC 346 MPG 324 from Evans et al. (2006); both spectra have been smoothed and rebinned to an effective resolving power of 4000. Emission lines identified in Sk 183 are N IV $\lambda\lambda 4058$; Si IV $\lambda\lambda 4089$, 4116; N III $\lambda\lambda 4634$ -41-42, with absorption from N V $\lambda\lambda 4604$, 4620. Absorption lines identified in MPG 324 are He I $\lambda\lambda 4388$, 4471, 4713; He II $\lambda\lambda 4026$, 4200, 4542, 4686. Both spectra show a combination of N IV emission and He I absorption inconsistent with a unique spectral type, suggestive of composite spectra. The gaps in the spectrum of MPG 324 are due to ‘hot’ pixels in the detector.

terminated iteratively, with the bolometric luminosity calculated from the absolute magnitude (-5.14 mag) from Section 3.1. The model spectra were convolved with a rotational-broadening function to take into account an apparent projected rotational velocity of $v \sin i = 60 \pm 20 \text{ km s}^{-1}$, determined from the metal lines (N III, N IV, N V, and Si IV). The primary temperature diagnostic available is the nitrogen ionization balance, with additional constraints given by the Si IV emission and the He I $\lambda 4471$ absorption.

From comparisons of model spectra with the observations, we adopted a nitrogen-rich model with $T_{\text{eff}} = 46 \pm 2 \text{ kK}$ and $\log g_{\text{eff}} = 4.0 \pm 0.1$, as shown in Figure 3. The stellar radius, at a Rosseland optical depth of 20, is $R_* = 9.7 R_{\odot}$. The He II $\lambda\lambda 4200$, 4542 lines were somewhat over-predicted by this model. While a cooler model ($T_{\text{eff}} = 42 \text{ kK}$) still provided a reasonable fit to the Si IV emission, it led to significant over-prediction of the He I absorption with little improvement for the He II lines. A simultaneous fit to the (notably broader) weaker He I lines was not possible with a model of a single star.

The adopted 46 kK model fits the observed N III, N IV, and N V features simultaneously with an abundance of $12 + \log([\text{N}/\text{H}]) = 7.73 (\pm 20\%)$. Compared with the Solar value of 7.83 (Asplund et al. 2009) this suggests significant enrichment compared to the baseline SMC value

found from H II regions (~ 6.55 , Russell & Dopita, 1990). The uncertainty quoted on the T_{eff} estimate ($\pm 2 \text{ kK}$) reflects the fitting of the stellar parameters. With more modest nitrogen abundances, e.g., a factor of two lower (comparable to that obtained for NGC 346 MPG 355 by Walborn et al. 2004), the N IV and N V features could be fit with a hotter temperature (of a few kK), but a simultaneous fit of the N III lines was not possible.

The mass-loss rate appears to be low, as might be expected given the reduced metallicity of the SMC (e.g. Bouret et al. 2003). We calculated a grid of models where all parameters were fixed, but with a range of $10^{-9} \leq \dot{M} \leq 10^{-5} M_{\odot} \text{ yr}^{-1}$. From comparison of the models with the observed spectra, $\dot{M} = 10^{-7} M_{\odot} \text{ yr}^{-1}$ was the best compromise to fit the observed UV (N v) and optical (H α and He II $\lambda 4686$) profiles. For example, if $\dot{M} > 10^{-7} M_{\odot} \text{ yr}^{-1}$ the predicted He II $\lambda 4686$ absorption was weaker than observed, suggesting this as an upper limit. A more precise estimate of \dot{M} would require high-quality UV and/or *K*-band spectroscopy.

To estimate v_{∞} we employed the empirical relation from Prinja (1994) between v_{∞} and the wavelength difference ($\Delta\lambda$) between the observed peak emission and minimum absorption of the N V or C IV lines in low-resolution *IUE* spectra. Using Prinja’s equation(1)

for Sk 183, $\Delta\lambda(\text{N V}) \approx 12 \text{ \AA}$, giving $v_\infty \approx 2150 \text{ km s}^{-1}$ ($\pm \sim 300 \text{ km s}^{-1}$); this value was adopted in our models.

The degree of clumping in the wind was poorly constrained by the available data because of the low mass-loss rate. The final model was therefore calculated without inclusion for the effects of clumping, but note that the exact values of v_∞ and the clumping factor did not have a significant impact on the other physical parameters. In particular, the N IV emission in our PoWR model does not arise from the wind, so was not affected by the adopted clumping factor.

When correcting the effective gravity for the contribution of radiation pressure we found $\log g = 4.11$, yielding a spectroscopic mass estimate of $M_{\text{spec}} = 46_{-8}^{+9} M_\odot$. This is in good agreement with the evolutionary mass obtained from comparisons with the theoretical evolutionary tracks for the SMC from Brott et al. (2011). For $v \sin i$ (init.) $< 350 \text{ km s}^{-1}$, the T_{eff} and L determined for Sk 183 lies roughly equidistant between the 40 and $50 M_\odot$ tracks, suggesting an evolutionary mass for Sk 183 of $45 \pm 5 M_\odot$, with a corresponding age of $\sim 2 \text{ Myr}$. In the LMC grid from Brott et al. there are also models for an initial mass of $45 M_\odot$. Scaling the moderate rotation models ($v \sin i$ (init.) $< 350 \text{ km s}^{-1}$) to the hotter temperatures obtained for stars in the SMC, we find reasonable agreement with the parameters obtained for Sk 183 (Dr I. Brott, private communication).

The parameters determined from the single-star analysis of Sk 183 are summarised in Table 3. For completeness, in the third column we provide the equivalent results assuming the canonical distance modulus to the SMC of 18.9 mag.

3.2.3. Composite Model

We also investigated a scenario in which the observed spectrum of Sk 183 is comprised of a hot O-type primary, combined with a cooler, lower luminosity, secondary component. Composite spectra were synthesized by scaling the continuum fluxes of the two components by their relative luminosities, such that the combined model reproduces the observed spectral energy distribution of Sk 183 (assuming a distance modulus of 18.7 mag). Given the large luminosity of the O3 component, the total contribution from, e.g., a B-type companion, is relatively small (indeed, it is within the uncertainty of the single-star fit).

Adopting the same radial velocity for the secondary spectrum, a reasonable fit was obtained with a composite of a slightly hotter, early O-type model ($T_{\text{eff}} = 47.5 \text{ kK}$) with that of an early B-type giant (with $\log L/L_\odot = 4.1$, $T_{\text{eff}} = 21 \text{ kK}$, and $\log g_{\text{eff}} = 3.5$), as shown in Figure 4. A large (projected) rotational velocity of $v \sin i = 250 \text{ km s}^{-1}$ was necessary for the secondary component to reproduce the broad He I lines.

While there is only tentative evidence of a secondary companion, we include this analysis to explore its potential consequences on the combined spectrum. Indeed, if a genuine binary, it would be surprising (in an evolutionary sense) to find a B-type giant with a much younger O3-type dwarf. However, this is not a unique solution for the secondary, as hotter models for the secondary (e.g. a late O-type star) also give reasonable fits.

The putative composite model has some advantages compared to the single-star fit. In addition to the fits

to the broad He I lines, the reproduction of the He II $\lambda\lambda 4200, 4542$ lines is improved due to dilution of the continuum level by the second component. Moreover, a more consistent fit is achieved for the He I $\lambda 4471$ line – we were unable to reproduce the broad wings and narrow core of this line simultaneously in the single-star model (see Figure 5). The parameters of the primary and secondary components in the composite model are summarised in Table 3.

4. DISCUSSION

The discovery of such an early-type star in the SMC, let alone in the Wing, is noteworthy. To place its rarity in context, there are published classifications for over 5000 luminous stars in the SMC (e.g. see compendium by Bonanos et al. 2010) but only two with secure spectral types of earlier than O4, namely NGC 346 MPG 355 and AzV 435¹¹. Thus, including the revised classification of MPG 324, the new spectroscopy of Sk 183 brings the total of O2 and O3 stars known in the SMC to only four objects.

These stars provide a glimpse of some of the most massive O-type stars in a very metal-poor environment, into a domain of significantly diminished mass-loss rates (e.g. Bouret et al. 2003). Indeed, in their discussions of chemically-homogeneous evolution in the context of gamma-ray bursts, Yoon et al. (2006) noted NGC 346 as the only obvious cluster in which to examine the evolution of the most massive stars in a truly metal-poor regime; Sk 183 provides an excellent additional case for further study. In particular, spectroscopic monitoring would be helpful to unveil its true nature.

4.1. Ionisation of the N90 Nebula

The *Spitzer* observations revealed a population of young stellar objects along the inner edge of the N90 nebula, with Carlson et al. (2007) concluding that star formation started in the central cluster $\sim 4 \text{ Myr}$ ago and has propagated outwards since then. The peak star formation rate in the region has occurred over the past 2.5 Myr (Cignoni et al. 2009), during which time it has been approximately constant (Carlson et al. 2011). The evolutionary age obtained for Sk 183 ($\sim 2 \text{ Myr}$, Section 3.2.2), is consistent with it forming in this recent phase of star formation. Meanwhile, the gas in the interior of the H II region is nearly quiescent and does not show violent motions (Nigra et al. 2008), leading Carlson et al. (2011) to conclude that photoionisation is the primary trigger of the current star formation.

N90 has been observed from the ground and with the *HST* in narrow-band filters, thus isolating the H α and [N II] emission. Using the ACS images obtained in program GO-10284 (P.I.: A. Nota) we integrated the flux from the high surface-brightness component of the nebula finding $\sim 2 \times 10^{-11} \text{ erg s}^{-1} \text{ cm}^{-2}$, after corrections for the foreground extinction and the weak [N II] emission. The former was taken as $A_R = 0.16 \text{ mag}$ from the NASA/IPAC Infrared Science Archive Extinction

¹¹ MPG 355 was classified as O2 III(f*) by Walborn et al. (2002) and ON2 III(f*) by Walborn et al. (2004); AzV 435 was classified as O3 V((f*)) by Massey et al. (2005). Note that the spectral type listed by Bonanos et al. for AzV 14 is O3-4 V (Garmany et al. 1987), but this was revised to O5 V by Massey et al. (2004).

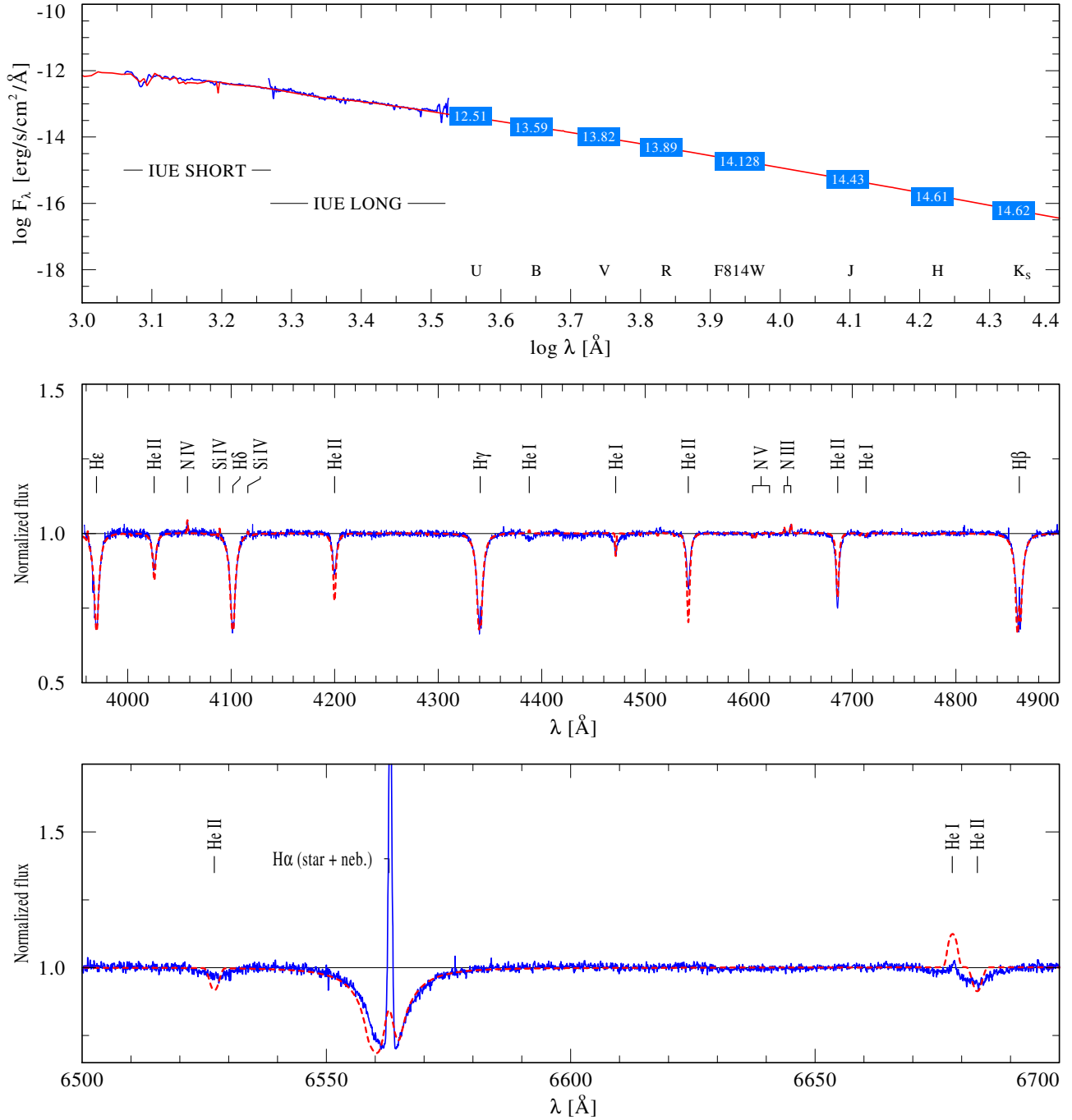


Figure 3. *Upper panel:* model fit to the spectral energy distribution of Sk 183, combining *IUE* spectroscopy and multi-band photometry as indicated. The total line-of-sight reddening, taking into account Galactic and SMC contributions, is $E(B - V) = 0.09$ mag. *Middle and lower panels:* comparison of the optical FLAMES spectrum of Sk 183 (blue solid line) with the adopted ‘single star’ PoWR model (red dashed line).

Calculator (which uses the results from Schlegel et al. 1998), while a contribution to the [N II] emission of 4% was adopted (e.g., Peña-Guerrero et al. 2012). However, the ACS image covers only the core part of N90, which extends over a larger area of $8' \times 6'$. Thus, integrating over the entire extent of N90 from the Magellanic Cloud Emission Line Survey (MCELS; Smith et al. 1999) we obtained $f_0(\text{H}\alpha) \approx 8 \times 10^{-11} \text{ erg s}^{-1} \text{ cm}^{-2}$ (cf. $f_0(\text{H}\alpha) = 10.8 \pm 1.1 \times 10^{-11} \text{ erg s}^{-1} \text{ cm}^{-2}$ from Kennicutt & Hodge, 1986). The flux from the MCELS image corre-

sponds to a total luminosity of $\geq 3.2 \pm 0.3 \times 10^{37} \text{ erg s}^{-1}$ (with the uncertainty indicative of the two distance moduli, i.e. 18.7 and 18.9 mag).

Converting this $L(\text{H}\alpha)$ to a Lyman continuum luminosity for a standard nebular case yields an ionization rate of $Q_0 \approx 2 \times 10^{49} \text{ s}^{-1}$. This will be a lower limit as some ionization surfaces within N90 are hidden from optical view by dark clouds and we have not accounted for leakage. Aside from Sk 183, the next earliest objects known in NGC 602a are stars #5 and #2 (Hutchings et

Table 3
Derived Properties of Sk 183

	Single-star Model		Composite Model	
	DM = 18.7 mag	DM = 18.9 mag	Pri.	Sec.
M_V	-5.14 mag	-5.34 mag	-5.14 mag	
$\log L/L_\odot$	5.58 ± 0.02	5.66 ± 0.02	5.57	4.1
T_{eff}		46 ± 2 kK	47.5 kK	21 kK
R_*	$9.7 R_\odot$	$10.7 R_\odot$	$9.6 R_\odot$	$8.5 R_\odot$
$\log g_{\text{eff}}$	4.0 ± 0.1	4.0 ± 0.1	4.0	3.5
$\log g$	$4.11^{+0.07}_{-0.08}$	$4.11^{+0.07}_{-0.08}$	4.11	3.5
M_{spec}	$46^{+9}_{-8} M_\odot$	$54^{+11}_{-7} M_\odot$	$40^{+8}_{-6} M_\odot$	$8.7 M_\odot$
\dot{M}		$10^{-7} M_\odot \text{ yr}^{-1}$	$10^{-7} M_\odot \text{ yr}^{-1}$...
$v \sin i$		$60 \pm 20 \text{ km s}^{-1}$	60 km s^{-1}	250 km s^{-1}
v_∞		$2150 \pm 300 \text{ km s}^{-1}$	2150 km s^{-1}	...
$\log Q_0$	49.37 s^{-1}	49.45 s^{-1}	49.41 s^{-1}	...
$12 + \log([\text{N}/\text{H}])$		$7.73 (\pm 20\%)$	7.73	...

Note. — The quoted errors on the single-star models are from fitting uncertainties. We do not quote uncertainties on the composite model as it is non-unique fit to the data.

al. 1991, classified as O8 and O9, respectively). The ionising fluxes from late O-type stars are over an order of magnitude lower (see, e.g., Smith et al. 2002), such that Sk 183 appears to be the dominant source of ionisation.

4.2. Mid-infrared Excess

The spectral energy distribution of Sk 183 is well matched in the near-IR by both the single-star and composite models (Figures 3 and 4). However, inspection of the new *WISE* photometry (Table 2) reveals an interesting upturn in the flux distribution, as shown in Figure 6. Observations with the short-wavelength *WISE* bands (*W1* and *W2*, corresponding to 3.6 and 4.6 μm , respectively) are in good agreement with the predicted flux from our PoWR models. But at the longer wavelengths of the *W3* and *W4* bands (12 and 22 μm), there is a clear mid-IR excess compared to the predicted distribution. A peak of the mid-IR flux distribution at 22 μm would argue for a blackbody temperature of order 130 K, or even cooler if the flux peaks at longer wavelengths.

Similar mid-IR excesses for otherwise normal OB-type stars have been seen in the SMC (Bolatto et al. 2007; Ita et al. 2010; Bonanos et al. 2010) and LMC (Evans et al. 2011). To investigate the mid-IR excess in Sk 183 further, we obtained images of the region from the *Spitzer* SAGE-SMC Survey (Gordon et al. 2011).

The InfraRed Array Camera (IRAC, 3.6, 4.5, 5.8, 8 μm) and Multiband Imaging Photometer for *Spitzer* (MIPS, 24 μm) images of Sk 183 are shown in Figure 7, together with an $\text{H}\alpha$ image obtained with the Mosaic II camera on the 4-m Blanco telescope at the Cerro Tololo Inter-American Observatory. From photometric extractions of the IRAC images we found: [3.6] = 14.75, [4.5] = 14.71, [5.8] = 14.67, and [8.0] = 14.66 mag. However, the peak of the 24 μm flux is offset slightly and appears extended (cf. the Airy rings seen around the point sources to the east), suggesting it as nearby dust emission, or unresolved dusty shocks (e.g. those seen in the Carina nebula, Smith et al. 2010), but not directly associated with Sk 183.

4.3. High-mass Star Formation in NGC 602

In the standard model of star formation, the initial mass function (IMF) is purely statistical in nature and

the probability of very massive stars being formed, while low, is independent of the mass of the star-forming region (e.g. Parker & Goodwin, 2007). In the integrated galactic IMF model (IGIMF, e.g., Weidner & Kroupa 2006) this probability increases with the mass of the star-forming region, with the prediction that the most massive stars should be found in the largest star-forming complexes.

NGC 602a is a relatively low mass cluster, with a stellar mass of $\sim 2000 M_\odot$ derived from the combination of the optical (Cignoni et al. 2009) and infrared imaging (Carlson et al. 2011). In this context, the IGIMF predictions from Weidner et al. (2011) suggest a maximum stellar mass of ~ 50 to $60 M_\odot$, roughly consistent with the estimated mass of the primary of Sk 183. Intriguingly though, Sk 183 is located approximately 45'' to the north-west of NGC 602a (corresponding to a projected distance of 12–13 pc, depending on the adopted distance modulus). This suggests the star has formed in *relative* isolation compared to the main body of the cluster (with no obviously massive cluster visible within 3 pc, e.g., Bressert et al. 2012), or that it is a slow runaway from NGC 602a, as alluded to by Gouliermis et al. (2012). Analysis of the line-of-sight velocities of other stars in N90 (and the gas profiles super-imposed on their spectra) is underway and should provide a more complete picture of the dynamics of this region.

While the single case of NGC 602 can not distinguish between the two IMF models, the SMC is rich in small, star-forming regions with masses in the range of 1000–2000 M_\odot . A more complete census of O-type stars in SMC clusters would provide an interesting test of the theories of the high-mass IMF, complementing recent work investigating ‘isolated’ O-type stars in the SMC by Lamb et al. (2010) and Selier et al. (2011).

ACKNOWLEDGEMENTS

Based on observations obtained in ESO program 086.D-0167. We are grateful to Nolan Walborn and Ines Brott for useful discussions, and to the referees for their constructive comments. We acknowledge DFG Grant OS 292/3-1 which supported a meeting of the authors, and LMO acknowledges DLR Grant 50 OR 1101. JSG thanks the University of Wisconsin-Madison Grad-

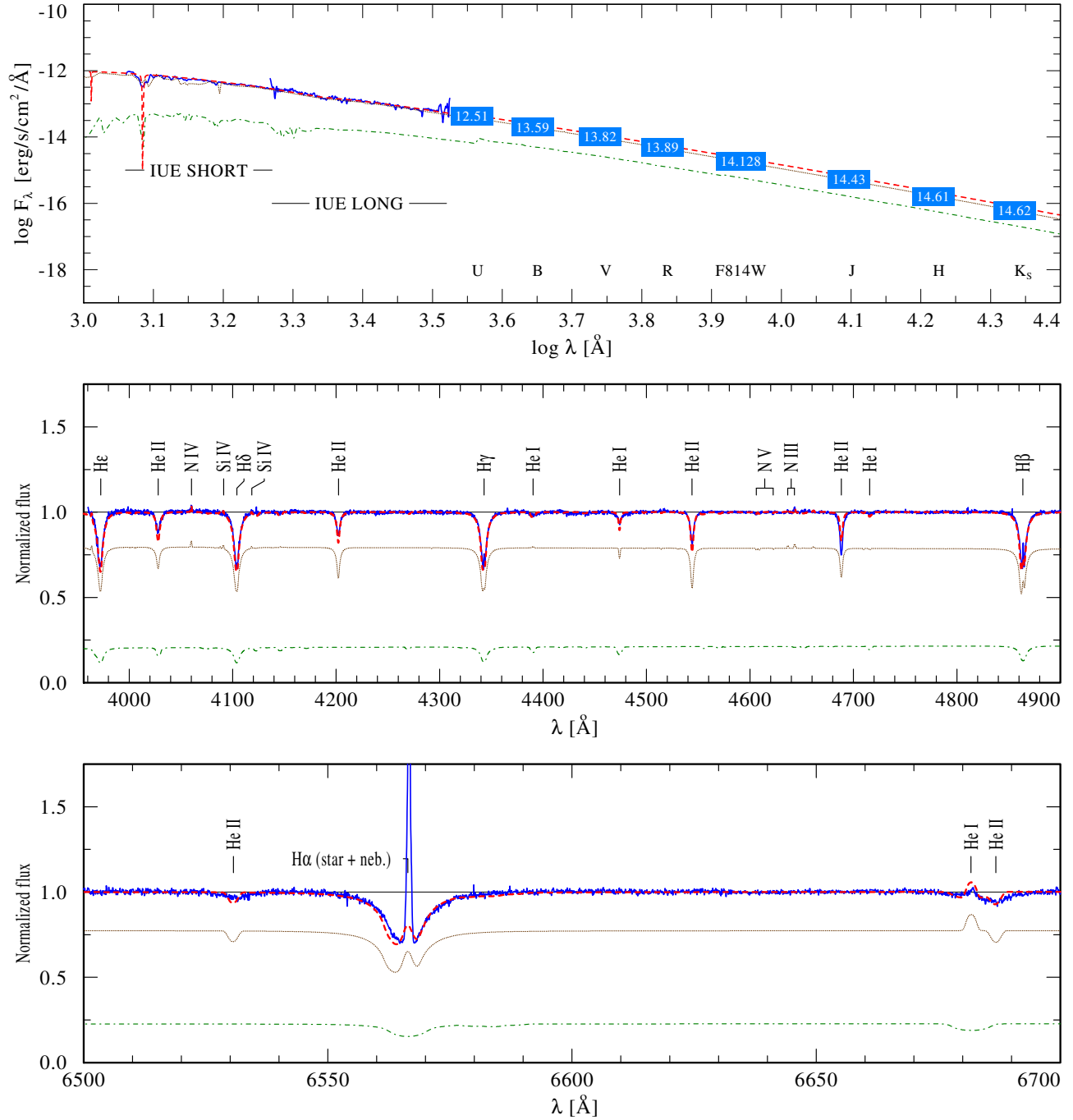


Figure 4. As Figure 3 but for a composite synthetic spectrum (dashed, red line), comprised of a hot O-type model ($T_{\text{eff}} = 47.5$ kK; dotted, brown line) and an early B-type component ($T_{\text{eff}} = 21$ kK; dash-dotted, green line). The latter two are plotted with their fluxes scaled by their relative intensities.

uate School for partial support of this work. JSG, YHC, and RAG are supported by the NASA Grant SAO GO0-11025X. VHB acknowledges support from the Scottish Universities Physics Alliance (SUPA) and from the Natural Science and Engineering Research Council of Canada (NSERC). This research has made use of the NASA/IPAC Extragalactic Database (NED) which is operated by the Jet Propulsion Laboratory, California Institute of Technology, under contract with NASA. This publication also makes use of data products from the *Wide-field Infrared Survey Explorer*, which is a joint

project of the University of California, Los Angeles, and the Jet Propulsion Laboratory/California Institute of Technology, funded by NASA.

REFERENCES

- Asplund, M. et al. ARA&A, 47, 481
 Bessell, M. S. 1991, A&A, 242, L17
 Bolatto, A. D. et al. 2007, ApJ, 655, 212
 Bonanos, A. Z. et al. 2010, AJ, 140, 416
 Bouchet, P. et al. 1985, A&A, 149, 330
 Bouret, J.-C. et al. 2003, ApJ, 595, 1182

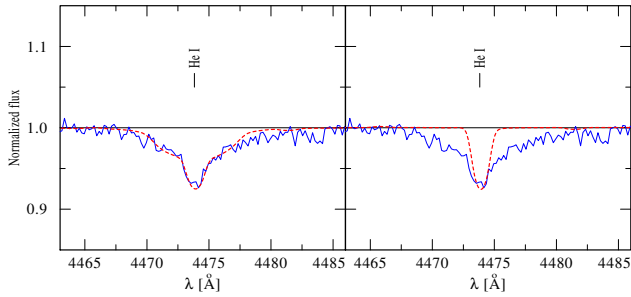


Figure 5. *Left-hand panel:* composite model (red; $T_{\text{eff}} = 47.5$ and 21 kK for the two components) of the observed He I $\lambda 4471$ profile. *Right-hand panel:* ‘single-star’ fit ($T_{\text{eff}} = 46$ kK).

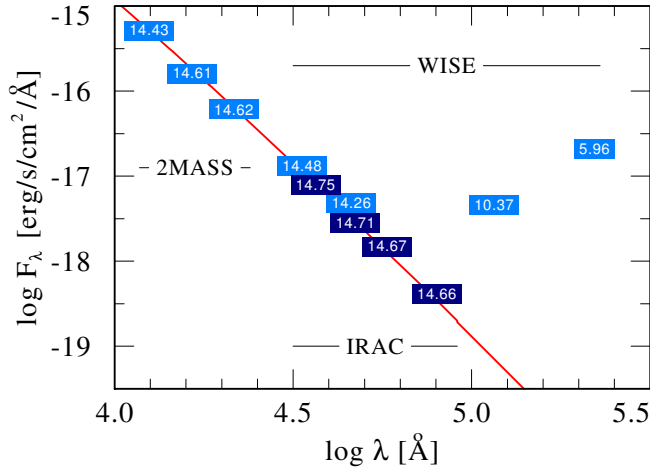


Figure 6. 2MASS, *WISE*, and *Spitzer*-IRAC photometry toward Sk 183, compared with the best fitting single-star model from Figure 3. The longer-wavelength *WISE* observations ($W3 = 12 \mu\text{m}$ and $W4 = 22 \mu\text{m}$) reveal an apparent mid-IR excess. Inspection of the *Spitzer* $24 \mu\text{m}$ image suggests that this excess arises from an extended source slightly offset from Sk 183 (see Figure 7).

Bressert, E. et al. 2012, *A&A*, in press, arXiv:1204.3628
 Brott, I. et al. 2011, *A&A*, 530, A115
 Carlson, L. R. et al. 2007, *ApJ*, 665, L109
 Carlson, L. R. et al. 2011, *ApJ*, 730, 78
 Cignoni, M. et al. 2009, *AJ*, 137, 3668
 Crowl, H. H. et al. 2001, *AJ*, 122, 220
 Evans, C. J., Lennon, D. J., Smartt, S. J. & Trundle, C. 2006, *A&A*, 456, 623
 Evans, C. J. et al. 2011, *A&A*, 530, A108
 Garmany, C. D., Conti, P. S. & Massey, P. 1987, *AJ*, 93, 1070
 Glatt, K. et al. 2008, *AJ*, 136, 1703
 Gordon, K. et al. 2011, *AJ*, 142, 102
 Gouliermis, D. A., Quanz, S. P. & Henning, T. 2007, *ApJ*, 665, 306
 Gouliermis, D. A. et al. 2012, *ApJ*, 748, 64
 Gräfenor, G., Koesterke, L. & Hamann, W.-R. 2002, *A&A*, 387, 244
 Hamann, W.-R. & Gräfenor, G. 2003, *A&A*, 410, 993
 Hamann, W.-R. & Gräfenor, G. 2004, *A&A*, 427, 697
 Harries, T. J., Hilditch, R. W. & Howarth, I. D., 2003, *MNRAS*, 339, 157

Henize, K. G. 1956, *ApJS*, 2, 315
 Hillier, D. J. & Miller, D. L. 1998, *ApJ*, 496, 407
 Howarth, I. D. 1982, *MNRAS*, 198, 289
 Howarth, I. D. 1983, *MNRAS*, 203, 301
 Hutchings, J., Thompson, I. B., Cartledge, S. & Pazder, J. 1991, *AJ*, 101, 933
 Ita, Y. et al. 2010, *PASJ*, 62, 273
 Jeffery, C. S. & Hamann, W.-R. 2010, *MNRAS*, 404, 1698
 Kennicutt, R. C. Jr & Hodge, P. W. 1986, *ApJ*, 306, 130
 Lamb, J. B., Oey, M. S., Werk, J. K. & Ingleby, L. D. 2010, *ApJ*, 725, 1886
 Lindsay, E. M. 1958, *MNRAS*, 118, 172
 Massey, P., Parker, J. W. & Garmany, C. D. 1989, *AJ*, 98, 1305
 Massey, P. 2002, *ApJS*, 141, 81
 Massey, P. et al. 2004, *ApJ*, 608, 1001
 Massey, P. et al. 2005, *ApJ*, 627, 477
 Massey, P. et al. 2009, *ApJ*, 692, 618
 Mathewson, D. S., Ford, V. L. & Visvanathan, N. 1986, *ApJ*, 301, 664
 Meaburn, J. 1980, *MNRAS*, 192, 365
 Niemela, V. S., Marraco, H. G. & Cabanne, M. L. 1986, *PASP*, 98, 1133
 Nigra, L. et al. 2008, *PASP*, 120, 972
 Oskinova, L. M., Feldmeier, A. & Hamann, W.-R. 2006, *MNRAS*, 372, 313
 Oskinova, L. M., Hamann, W.-R. & Feldmeier, A. 2007, *A&A*, 476, 1331
 Oskinova, L. M. et al. 2011, *MNRAS*, 416, 1456
 Parker, R. J. & Goodwin, S. P. 2007, *MNRAS*, 380, 1271
 Pasquini, L. et al. 2002, *Msngr*, 110, 1
 Peña-Guerrero, M. A. et al. 2012, *ApJ*, 746, 115
 Prinja, R. K. 1994, *A&A*, 289, 221
 Puls, J. et al. 2005, *A&A*, 435, 669
 Putman, M. E. 2000, *PASA*, 17, 1
 Rivero González, J. G. et al. 2011, *A&A*, 536, A58
 Russell, S. C. & Dopita, M. A. 1990, *ApJS*, 74, 93
 Sanduleak, N. 1969, *AJ*, 74, 877
 Schlegel, D. J., Finkbeiner, D. P. & Davies, M., 1998, *ApJ*, 500, 525
 Schmalzl, M. et al. 2008, *ApJ*, 681, 290
 Selier, R., Heydari-Malayeri, M. & Gouliermis, D. A. 2011, *A&A*, 529, A40
 Skrutskie, M. F. et al. 2006, *AJ*, 131, 1163
 Smith, L. J., Norris, R. P. F. & Crowther, P. A. 2002, *MNRAS*, 337, 1309
 Smith, N. et al. 2010, *MNRAS*, 406, 952
 Smith, R. C. et al. 1999, in *IAU Symp. 190, New Views of the Magellanic Clouds*, ed. Y.-H. Chu, N. Suntzeff, J. Hesser & D. Bohlender, 28
 Sota, A. et al. 2011, *ApJS*, 193, 24
 Walborn, N. R. et al. 1995, *PASP*, 107, 104
 Walborn, N. R. & Blades, J. C. 1997, *ApJS*, 112, 457
 Walborn, N. R. et al. 2000, *PASP*, 112, 1243
 Walborn, N. R. et al. 2002, *AJ*, 123, 2754
 Walborn, N. R. et al. 2004, *ApJ*, 608, 1028
 Walborn, N. R. in *From Pop III and GRBs to the Milky Way. STScI Symp. Series No. 20*, ed. M. Livio & E. Villaver. Cambridge University Press, 2009, 167
 Weidner, C. & Kroupa, P. 2006, *MNRAS*, 365, 1333
 Weidner, C., Pflamm-Altenburg, J. & Kroupa, P. 2011, in *UP2010: Have Observations Revealed a Variable Upper End of the Initial Mass Function?* ed. M. Treyer, K. Wyder, J. D. Neill, M. Seibert & J. C. Lee, ASP Conf. Ser. 440, 19
 Westerlund, B. E. 1964, *MNRAS*, 127, 429
 Wright, E. L. et al. 2010, *AJ*, 140, 1868
 Yoon, S.-C., Langer, N. & Norman, C., 2006, *A&A*, 460, 199

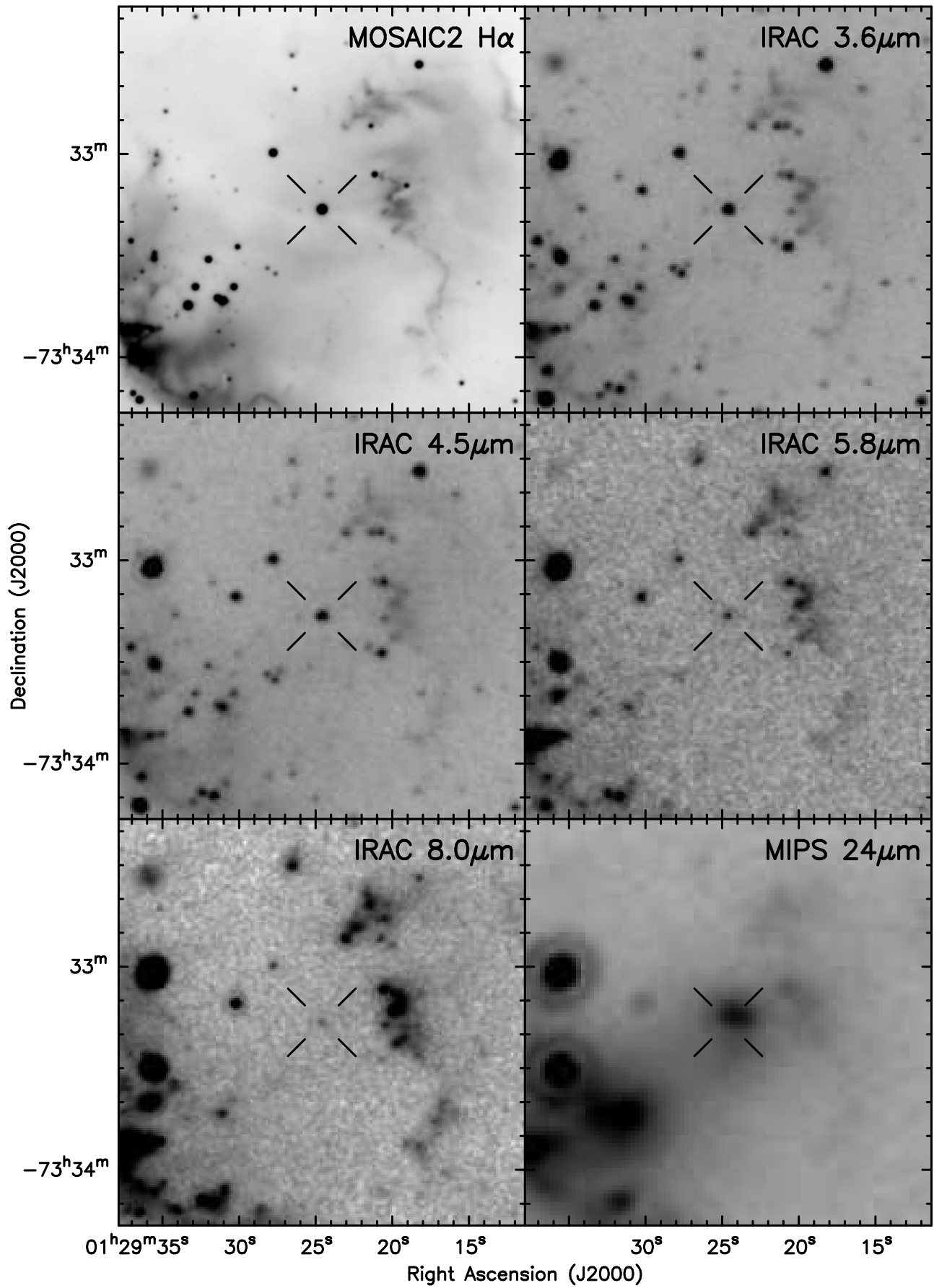


Figure 7. MosaicII ($H\alpha$), *Spitzer* IRAC, and MIPS ($2' \times 2'$) images of Sk 183 (marked by the open cross) and the surrounding nebula. In the MIPS $24\mu\text{m}$ image the mid-IR excess emission suggested by the *WISE* photometry (see Section 4.2) appears to arise from an extended source slightly offset from the location of Sk 183.